A technique to measure optical properties of brownout clouds for modeling terahertz propagation

Steven T. Fiorino,[1,*] Jason A. Deibel,[2,3] Phillip M. Grice,[1] Markus H. Novak,[1] Julian Spinoza,[1] Lindsay Owens,[2] and Satya Ganti[3]

[1]Center for Directed Energy, Air Force Institute of Technology, 2950 Hobson Way, Wright-Patterson Air Force Base, Ohio 45433-7765, USA

[2]Department of Physics, Wright State University, 3640 Colonel Glenn Highway, Dayton, Ohio 45435, USA

[3]Department of Electrical Engineering, Wright State University, 3640 Colonel Glenn Highway, Dayton, Ohio 45435, USA

*Corresponding author: steven.fiorino@afit.edu

Received 3 January 2012; revised 11 March 2012; accepted 23 March 2012; posted 29 March 2012 (Doc. ID 160548); published 1 June 2012

Brownout, the loss of visibility caused by dust resultant of helicopter downwash, is a factor in the large majority of military helicopter accidents. As terahertz radiation readily propagates through the associated dust aerosols and is attenuated by atmospheric water vapor within short distances, it can provide low-profile imaging that improves effective pilot visibility. In order to model this application of terahertz imaging, it is necessary to determine the optical properties of obscurants at these frequencies. We present here a method of empirical calculation and experimental measurement of the complex refractive index of the obscuring aerosols. Results derived from terahertz time-domain spectral measurements are incorporated into the AFIT CDE Laser Environmental Effects Definition and Reference (LEEDR) software. © 2012 Optical Society of America

OCIS codes: 040.2235, 290.5820, 010.1110.

1. Introduction

The Air Force Institute of Technology Center for Directed Energy (AFIT CDE) has developed modeling code to simulate the operating conditions associated with the use of terahertz imaging in brownout conditions. The Laser Environmental Effects Definition and Reference, or LEEDR [1], code allows the export of first principles atmospheric characterizations for use in other simulation codes, military or Department of Defense (DOD) mission planning, or even nonmilitary scientific research such as climate change impact studies. A recently implemented capability within LEEDR allows the calculation of optical transmission through simulated rotary-wing brownout conditions at both desert and mid-latitude land sites throughout the world based on an internal climatological database. The accuracy of the LEEDR model is dependent on *a priori* understanding of the interaction of light at a given frequency with its surrounding medium and the dirt aerosols in brownout conditions. Thus, the effectiveness of the LEEDR code is bolstered by experimental verification of the complex refractive index of the interaction medium at the operational optical frequencies.

Terahertz radiation is customarily defined as the far-infrared (FIR) electromagnetic radiation between about 100 GHz and 10 THz. This frequency range was largely unexplored until two decades ago [2] when a series of technological developments [2–4] allowed for the generation and detection of terahertz waves in a practical and reliable fashion. The appeal of utilizing terahertz radiation for sensing and imaging purposes is further enhanced by the fact that many dielectric materials are either transparent or only slightly absorbing at these frequencies. Terahertz time-domain spectroscopy (THz-TDS), with its broad fractional bandwidth and subpicosecond time resolution, offers an effective method of characterizing a substance's

1559-128X/12/163605-09$15.00/0

frequency-dependent absorption and refractive index.

The use of terahertz imaging for brownout situations is even more appealing when its inability to propagate over large distances in the atmosphere is considered. While for many applications this would be seen as detrimental, in this one it is advantageous. The terahertz light is efficiently absorbed by atmospheric water vapor, such that it is attenuated below typical detection levels within relatively short distances from the brownout event. This allows it to be used in covert situations—something unavailable to more conventional radar imaging systems.

The remainder of this paper is organized as follows. First, the LEEDR algorithm used to model the transmission of light through brownout conditions is described. This is followed by a discussion of transmission and scattering measurements on various sand configurations, performed using terahertz time-domain spectroscopy systems. The paper concludes with an analysis of how the experimental results compare with the transmission and scattering results obtained from the brownout model.

2. Brownout Model Description

The purpose of this project was to validate LEEDR's model of the propagation of terahertz radiation through brownout conditions via comparisons to transmission properties derived from experimental measurements, namely terahertz time-domain spectroscopy. The existing model, implemented by Marek [5], utilizes an assumed particle distribution, number concentrations, and extrapolated optical property values for mid-latitude and desert brownout cloud particles. Results reported here were resultant from a new version of the model that allows for the input of laboratory-measured extinction values to directly obtain complex index of refraction values rather than extrapolated values. Using these inputs, LEEDR creates profiles of altitude versus absorption, as well as transmission versus wavelength. Figure 1 shows how climatological inputs can be specified by the Extreme and Percentile Environmental Reference Tables (ExPERT) database. LEEDR uses the ExPERT database to provide climatological profiles of temperature, humidity, and wind speed at varying altitudes in the atmosphere. LEEDR's output allows the user to examine values such as path transmittance, path extinction, and specific attenuation. The combination and integration of the aforementioned models with the LEEDR software couple these algorithms with a worldwide environmental effects characterization capability. Previously, this combination had not been quantified with an actual distribution of environmental brownout particles.

3. Laboratory Measurements and Incorporation into the Model

A. Technical Approach

Initial optical properties for the brownout particle distribution in LEEDR utilized published data at a

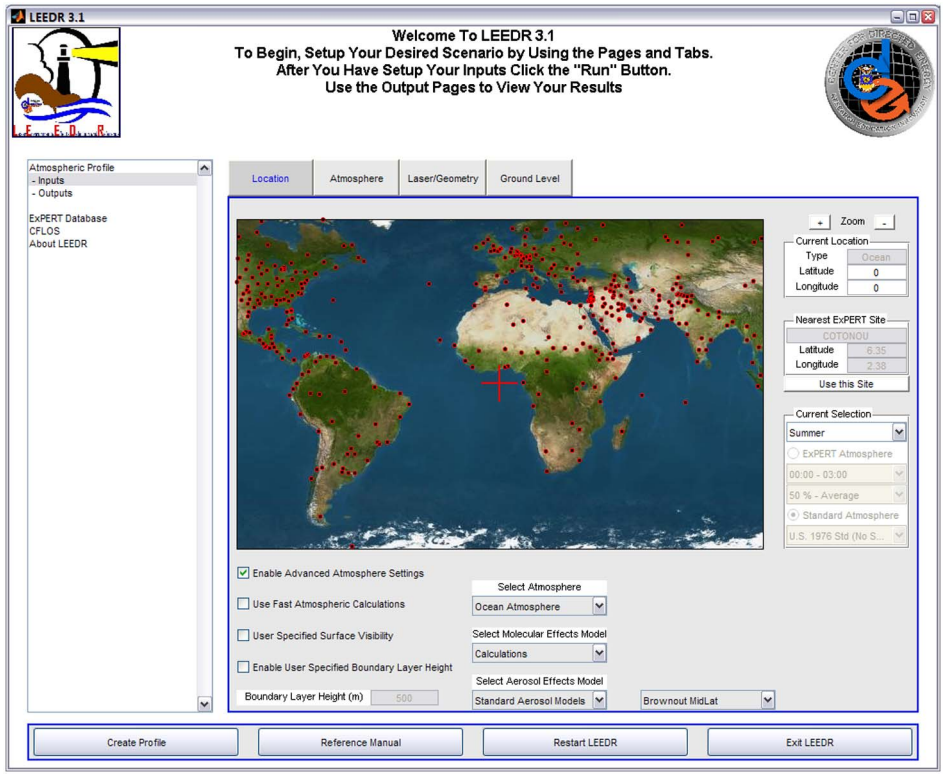

Fig. 1. (Color online) The LEEDR 3.1 input GUI. The user is able to define various scenarios and environmental conditions. Dark circles on the map represent ExPERT sites.

wavelength of 40 μm, documented in [5,–7], and experimentally determined properties for silica [8]. The detailed silica data were used to extrapolate the optical properties of brownout aerosols at wavelengths from 40 μm out to 3 mm, by maintaining the rate of change observed in the refractive index of silica in the same frequency range. This estimation is explained in more detail elsewhere [5,6]. In order to improve the model, this research sought to develop a technique to determine the brownout optical properties (or complex index of refraction, CIR) experimentally for wavelengths in the terahertz portion of the spectrum (0.1–3 THz).

The initial proposed method was to measure the extinction caused by a thin dirt sample of well-known composition. In order to avoid multiple scattering, which could cause unanticipated direct transmission values given an assumption of single scattering, a filtered monolayer was used for each of the samples. Knowing the physical properties of the dirt in the sample, including the number and size of the grains, LEEDR was used to complete Mie scattering calculations [9]. These calculations utilize the known physical parameters, in conjunction with the existing optical properties (as determined by [5,6]), to calculate the scattering, absorption, and thereby extinction that that sample should cause.

Assuming that the empirical and calculated values differ, the optical properties are then varied until the extinctions match. At that point where these values match, the model accurately predicts the extinction caused by brownout-like particles, and so the correct optical properties have been determined. A schematic of this method is shown in Fig. 2. For this experiment to work, however, it is necessary to assume that the real portion of the complex index of refraction can be determined from reference, such that we need only alter the imaginary component to adjust absorption to the necessary levels. However, the results of the experiment suggest that this is not the case and that additional information is necessary to fully and accurately determine the complex index of refraction.

B. Direct Transmission Measurements

Initially, transmission measurements were undertaken using the Bruker-80 v FTIR spectrometer, but these data proved not to be very useful, as only a small portion of its tunable range of ~15–30 μm contained a strong enough signal to penetrate the sample. Data in this spectral range overlapped with existing properties in LEEDR and provided no new information. Additional transmission measurements were completed using a terahertz time-domain spectrometer (TDS) configured in a transmission geometry [10,11]. Subpicosecond terahertz pulses were generated by exciting a GaAs photoconductive antenna with 100 fs long pulses from a Ti:Sapphire ultrafast laser and detected using a low-temperature-grown (LTG) GaAs receiver antenna that was gated by pulses from the same laser. The terahertz pulses were focused onto the samples with a 50.8 mm diameter, 120 mm focal length high-density polyethylene (HDPE) lens and then collected with a second identical lens. The typical bandwidth of the system, taken when the pulse propagated through air, spanned from 0.05 to 1 THz. Transmission measurements were performed on large samples (240–550 μm diameters) and small samples (177–240 μm diameters) of sand in which the particles were held in place using cellophane tape. Reference measurements were completed using tape samples devoid of any sand, and little to no pulse attenuation or dispersion was observed.

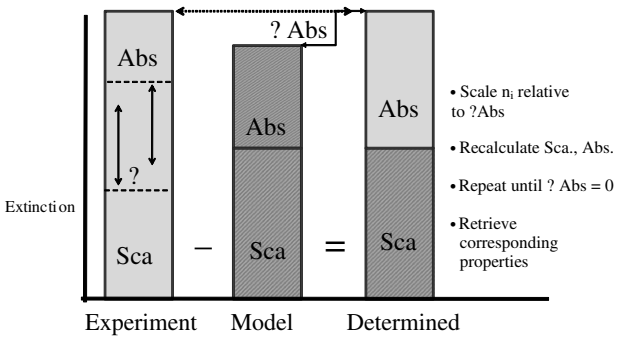

Fig. 2. Schematic of method used to determine optical properties from extinction.

One of the reasons that THz-TDS is an attractive technique for measurements such as those described here is that the electric field is measured as a direct function of time, allowing for both the spectral amplitude and phase of the pulse to be deduced via fast Fourier transform (FFT) of the time-domain data. A basic terahertz spectroscopy experiment involves placing a sample in the terahertz beam path; the time-resolved terahertz pulse is then compared with a reference pulse obtained in the absence of a sample. Extraction of the complex refractive index from the time-domain data is accomplished by comparison of the transmitted (or reflected) complex spectrum, obtained via FFT, of the pulse that interacted with the sample to the spectrum of the reference pulse that traveled through air or vacuum. This complex transmittance (or reflection) function is compared with the Fresnel conditions for transmission or reflection at the sample interfaces.

In this study, two methods were employed to analyze the transmission data taken using the THz-TDS system. The first method involved creating a special interface within LEEDR to evaluate the experimentally determined extinction against the calculated Mie scattering to determine the absorption component. The inputs include particle number concentration, particle size range, sample thickness, and empirical extinction. This resulted in output from LEEDR that included complex index of refraction, cloud visibility, and extinction coefficients. However, this method assumed that the real index is known from previous research, i.e., the real index of silica from reference [8]. The results using this method as applied to the data collected in transmission using

the THz-TDS system are plotted for the desert case in Fig. 3 [10]. Clearly, the absorption components seem artificially low at most of the frequencies sampled. In general, when the extinction is relatively high, high values of both the real and imaginary index are deduced. When measured extinctions are relatively moderate or low, the deduced absorption is found to be near zero. It appears that the assumption that the real index is very close to previously published values may be incorrect—making this a univariate solution to a bivariate problem [10].

In the second method, the frequency-dependent complex refractive index was calculated using the previously described method [12,13]. In order to arrive at an experimental value for the complex index, it is necessary to determine the real part of the refractive index (phase delay) and the imaginary part via the absorption coefficient. The real part of the refractive index is arrived at by determination of the difference in accumulated phase as compared between the sample and reference data. Likewise, the absorption coefficient is calculated by comparison of the two spectral amplitudes. The real part of the refractive index is utilized in the absorption coefficient calculation in order to account for any Fresnel loss at the air-sample interfaces. This series of calculations required a number of assumptions, which made these values suspect outside of the 0.1 to 1 THz range. The suspicion placed on these values motivated the design of the broad-spectrum extinction method in the first place. However, the results with the second method provided more reasonable values in the 0.1 to 1 THz portion of the spectrum (Figs. 4[a] and 4[b]) [10].

C. Scattering Measurements

As the direct transmission measurements did not provide the necessary information, a further experiment was designed, through which both absorption and scattering, and thereby the full complex refractive index, could be determined. This approach functioned by measuring the scattering directly across a range of angle increments from the sample.

As with the transmission measurements described in Subsection 3.B, a terahertz time-domain spectrometer was used for this experiment. These scattering measurements were performed with a more advanced terahertz system (Teraview) that provided in excess of 3 THz of bandwidth. Terahertz pulses

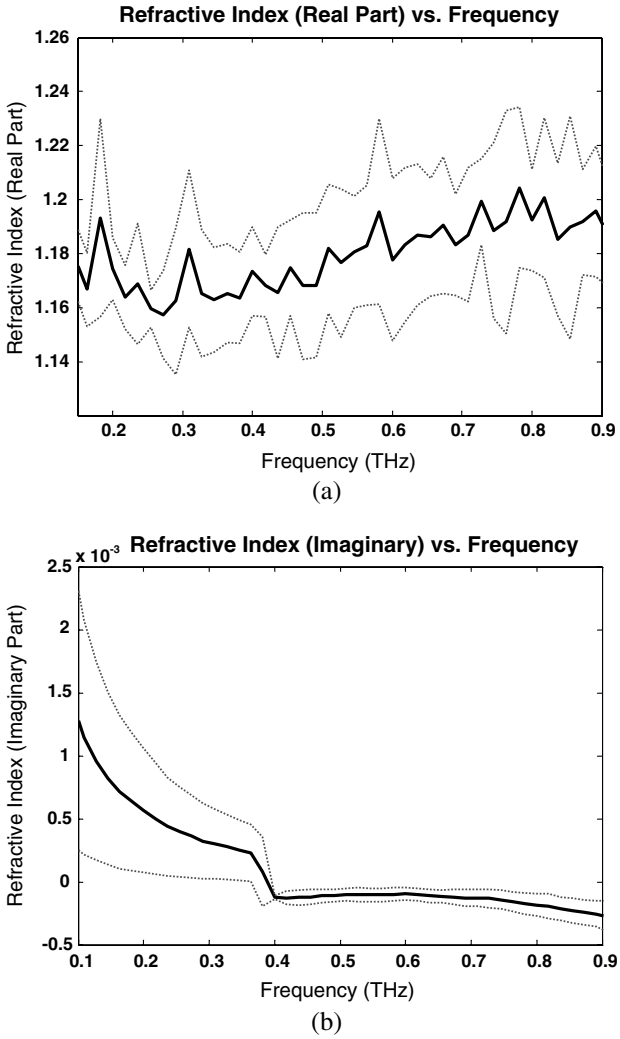

Fig. 4. (a) Real portion of the refractive index was found to be between ~1.1 and ~1.2; the previous model suggested a real index value between 2.3 and 2.4. Dotted lines show ±1 standard deviation. (b) Imaginary portion of refractive index, data filtration during calculation results in a smooth, piecewise curve. Discontinuity at $f = 0.4$ is likely a calculation artifact. Dotted lines show ±1 standard deviation.

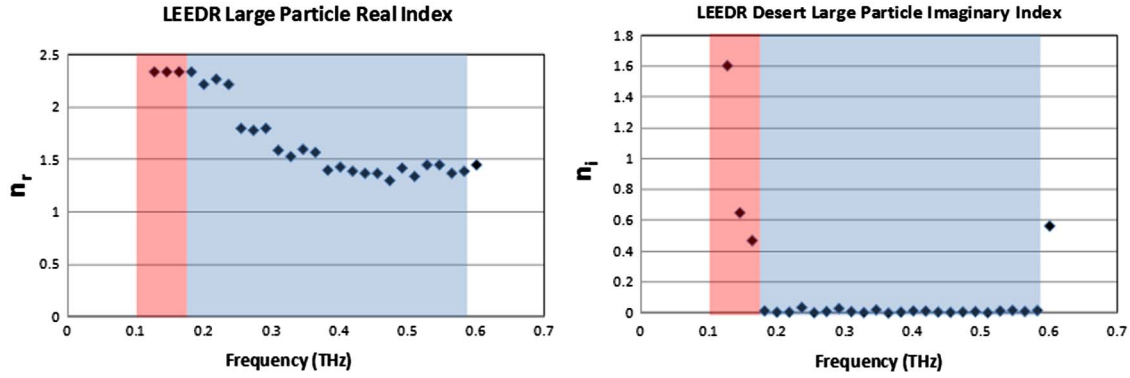

Fig. 3. (Color online) Extinction evaluation results, using real index from reference.

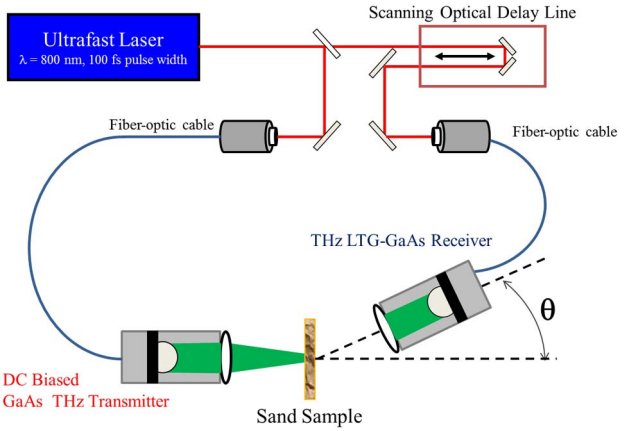

Fig. 5. (Color online) Schematic of off-axis terahertz time-domain spectrometer measurements.

were generated from a fiber-coupled GaAs photoconductive antenna and focused using a 25.4 mm diameter, single-crystal quartz 50 mm focal length lens, and detected with a fiber-coupled LTG GaAs antenna. Both antennas were driven by a 100 fs ultrafast laser. Given that the terahertz emitter and receiver are based on photoconductive dipole antennas, the polarization in this setup was inherently linear in nature [14]. In the case of the scattering measurement setup described below and in Fig. 5, the emitter antenna was oriented such that the dipole generated THz pulses that were primarily *p* polarized (horizontal) and the receiver antenna was oriented for detection of *p*-polarized light. Studies have shown while photoconductive antennas do not emit a purely linearly polarized pulse, the orthogonal polarization component is no more than 7% of the primary polarization. Consequently, photoconductive receiver antennas are very insensitive in terms of detecting light polarized orthogonally to the direction of the dipole antenna. Hence, for this work, it is a valid assumption that the incident THz pulses were *p* polarized and that all detected THz pulses were *p* polarized as well.

For each sample, a series of measurements was made to determine the magnitude of the normally incident terahertz pulse after having traveled through the sample. In each measurement set, the receiver was rotated away from the central axis created by the emitter and sample, to the point where it no longer measured the original signal. This experimental modality characterized the portion of the signal scattered away from its initial path by the sample. Thus, the scattering angle is defined as the angular displacement between the central axis and the placement of the receiver. A diagram of this system can be seen in Fig. 5, where θ represents the scattering angle. It can be assumed in all subsequent plots and figures in this paper that θ is the scattering angle. Representative waveforms acquired using this system are shown in Fig. 6, in which both time-domain and the resulting frequency-domain data are shown for transmission through air at "zero" angle detection, through sand at "zero" angle detection, and finally through sand at a detection or scattering angle of 20°. These plots also demonstrate the excellent signal-to-noise-ratio and bandwidth provided by the system.

As before, LEEDR was used to perform Mie scattering calculations, with modifications to the interface to allow the physical and optical properties to be varied. Within LEEDR, the results of the calculations are also converted into a scattering phase function representing the expected angle-dependent experimental results based on the given properties. The generated and empirically determined phase functions were compared and the sample parameters varied until the two functions matched. When and if the phase functions matched, it meant that the model accurately predicted both the absorption and scattering of the incident beam. This means the input parameters are representative of the sample's actual physical properties, including the CIR.

Six different sand samples were created for testing. Each was a monolayer of sand held to a packing tape layer, which was largely transparent to terahertz radiation, and held in a frame during testing. Each type of sand was analyzed under a microscope to determine its average particle size. An example of this is shown in Fig. 7. The range of particle sizes for each sample is shown in Table 1. Transmission data were gathered for all six collected samples, but scattering data were gathered for only four of the six. The four normalized off-axis data sets are shown in Fig. 8.

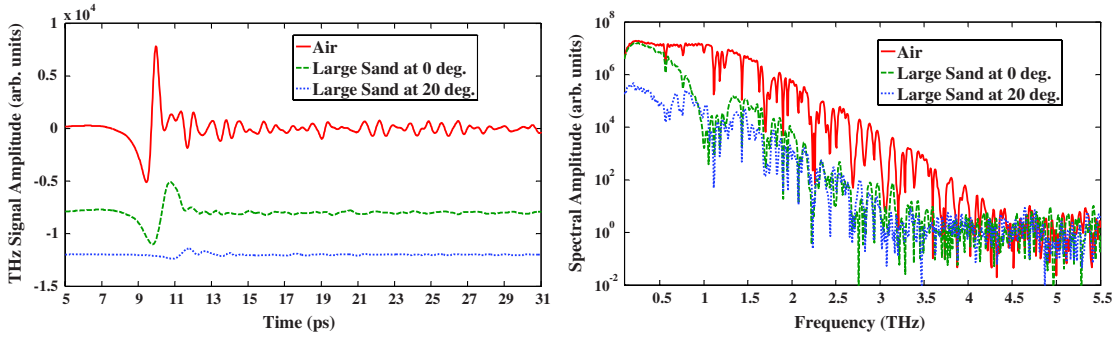

Fig. 6. Representative time-domain (left) and frequency domain (right) data taken using the off-axis terahertz time-domain spectrometer measurements.

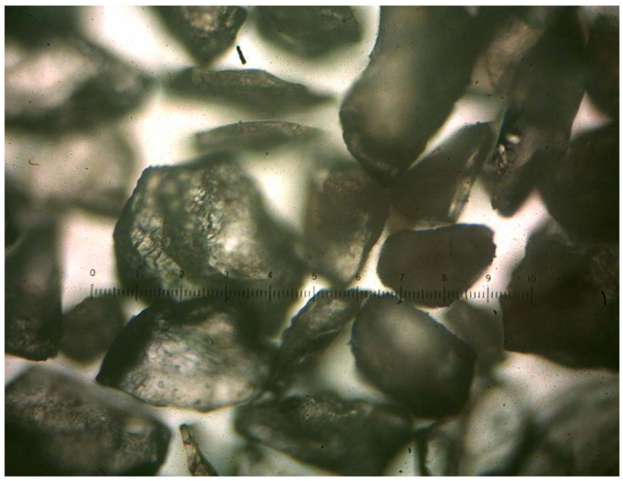

Fig. 7. (Color online) Large sand particles, as observed under a microscope.

The four data sets were then processed using Eq. (1), and the resultant data plotted. In Eq. (1), R = path length, β = scatter coefficient, I_{SCA} = measured spectral amplitude, I_0 = initial spectral amplitude, and d_v = volume increment:

$$p(\theta) = \frac{4\pi R^2 I_{\mathrm{SCA}}}{\beta I_0 d_v}. \quad (1)$$

These plots, shown in Fig. 9, are three of the empirically determined phase functions that all following LEEDR calculations will be compared against. Figure 9 also includes a scattering phase function calculated from the default brownout values, as determined by [6] and [8]. Note that the gray-shaded lines correspond to measurements taken at 1.0 THz; measurements taken at different frequencies cannot be compared, as wavelength has a large impact on the shape of the phase function. Comparing the initial calculated and empirical functions, it is apparent that they have little in common. This means the default brownout parameters do not accurately describe the physical sample. Ideally, the generated phase function would mimic the shape and magnitude of those constructed from the collected data. Effecting this change in the generated phase functions is the objective in this portion of the research.

In order to alter the properties of the model, the LEEDR code and GUI were modified. Previously, the brownout model was a static option in which the parameters were hardcoded; changes to the GUI allow the user to specify the properties of the model's constituent particles. These properties include real and imaginary components of the complex index of refraction, particle concentration, as well as minimum and maximum particle radii. The altered GUI is shown in Fig. 10. Further, the Mie scattering module of the LEEDR code was modified to accept these fields as variable inputs, allowing the parameters to be taken into account in the scattering equations, while preventing them from becoming mandatory inputs for a conventional LEEDR application. Aside from this research, this modified version of LEEDR is a useful tool, allowing an arbitrary sample phase function to be correlated to physical properties, and will remain available for any future investigations.

Table 1. Sample Particle Sizes

Sand Sample	Size Range (μm)
Small sand	70–320
Large sand	50–650
Iraq	1–250
YPG, unfilitered	4–200
YPG, filtered	5–150
Gray powder	1–300

Effects of variations in each of the parameters were recorded, as is shown in Fig. 10. Varying the properties individually allows their influence on the shape of the phase function to be interpreted independently. The first property analyzed was particle size, as it was noted that the default model assumed the presence of smaller particles than were actually being found in brownout scenarios. This also served to test and debug the modifications. As can be seen in the upper-left plot of Fig. 11, increases in constituent particle size lead to an increase in amplitude at the smaller scattering angles. Additionally, as the average particle size was increased, the phase function began to develop a characteristic secondary peak—a feature observed in the empirical functions. Variations in the complex index of refraction proved to induce more subtle changes. The two rightmost plots show these effects. However, the real and imaginary indices are partially codependent, as noted in the method outlined in Fig. 2. The bottom-left plot is another example of variations in the imaginary index, but evaluated at a lower real index; comparison of the lower two plots reveals an influence of the real index on changes in the imaginary.

One notable, though consistent, feature of the empirical phase functions (Fig. 9) is the precipitous drop-off observed as the phase angle approaches 50°. This is believed to be the result of a loss of sensitivity in the instrumentation at such low intensities. Nonetheless, it implies low phase function values at higher phase angles. This is observed in Fig. 11 for low real and imaginary indices. Altering the particle concentration was not found to have any significant effects.

An effect not captured in the experiments described above is polarization. In general small-particle aerosol scattering in the visible and near infrared is dominated by the forward scattering peak, and this causes the degree of polarization to be negligible at small scattering angles [15]. Brownout scattering of submillimeter energy has a similar particle size to energy wavelength ratio as small-particle aerosols to visible light and has a similar forward scattering peak as shown in Fig. 11. Thus it is expected that the degree polarization in the experiments outlined

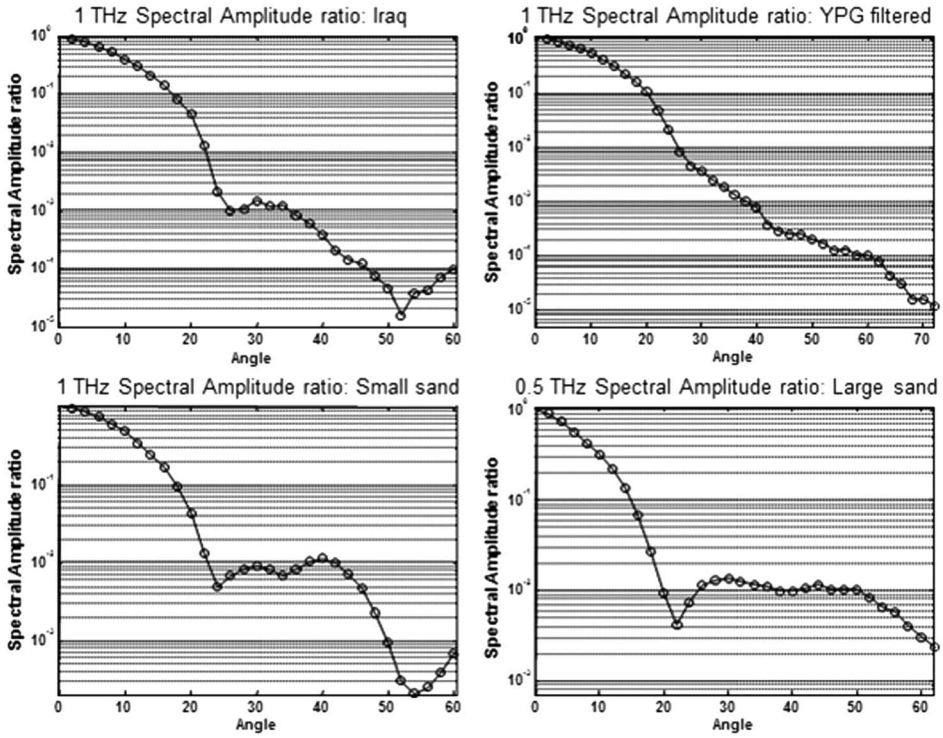

Fig. 8. Off-axis spectral amplitude ratios collected through a range of angle increments, for four samples.

above is not significant out to the off-axis angles measured of 50° to 60°.

As is the case with any experimental determination of physical constants, it is important to consider any errors inherent to the measurement process. While terahertz time-domain spectroscopy is a relatively young technique, work has been done to analyze measurement uncertainty and error sources associated with the determination of optical parameters using THz-TDS [16]. Dominant sources of error in time-domain spectroscopy measurements include fluctuations in the amplitude of the pulse, errors associated with sample thickness determination, noise, and scattering. Typical THz-TDS experiments are conducted in a transmission or specular reflection modality that ignores angular-dependent scattering issues. As the work presented in this paper in fact measured such, the results are immune from error due to neglecting scattering issues. In regard to errors introduced by pulse amplitude fluctuations and noise, their origin is tied to the terahertz system employed for the measurements. In the case of this work, a commercial THz-TDS system was used, which was driven by a stabilized ultrafast laser. This commercial terahertz system exhibited excellent pulse-pulse stability and has operated with effectively no pulse amplitude fluctuations for time periods greater than 36 h. In order to minimize what little fluctuations and noise were present, signal averaging was employed. Issues associated with sample thickness errors were discussed previously in terms of the influence of the sample particle size (Fig. 11).

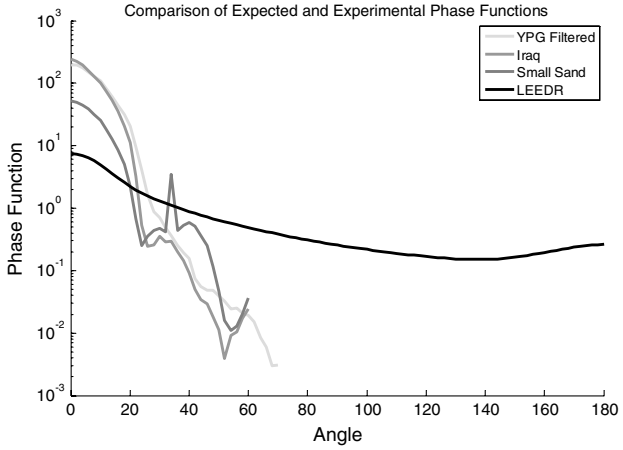

Fig. 9. Three laboratory-measured and initial calculated phase functions. All phase functions evaluated at 1 THz.

Through a combination of variations in the model's properties, a close match in computed and measured phase functions was determined (Fig. 12). Comparing Figs. 9 and 12, it is apparent that the new model far surpasses the old in accurately describing the scattering produced by a sample. This means the specified parameters more accurately describe the physical properties of the sample. As such, this approach successfully determines the optical properties of the sampled obscurant. This plot implements a particle size range of 325–425 μm, and a complex index of refraction of 1.2 – 01i, whereas the previous model used particles of size 1–500 μm, with a CIR of 2.34 – 0.08i. The change in average particle size reflects the larger expected particles in brownout

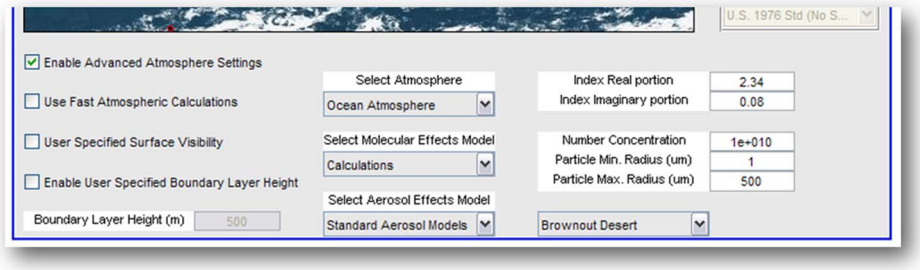

Fig. 10. (Color online) A portion of the modified LEEDR GUI, including five new input fields corresponding to the sample parameters.

scenarios. Further, the newly determined scattering (real) coefficient agrees with the results obtained using the method described in Subsection 3.B, while maintaining a realistic absorption component.

4. Summary

The AFIT CDE has developed a tool to evaluate terahertz propagation and imaging through brownout conditions. The molecular and aerosol absorption and scattering effects have been shown and evaluated in the brownout environment. While the aerosols prove to be the dominating effect at longer wavelengths, the ability to transmit through a representative brownout environment can be achieved at the wavelengths researched. In order to further investigate aerosol effects in this frequency range, simple desert and midlatitude brownout aerosol models were constructed in LEEDR, based on an experimental study by the Midwest Research Institute, which was able to quantify the particle concentration that exists in rotary-wing brownout conditions.

Initially, to improve the brownout characterizations within LEEDR, laboratory measurements of on-axis extinction at THz wavelengths through monolayers of various desert sands were made. These measured values allowed the deduction of optical properties to include both scattering and absorption coefficients. Transmission data were analyzed using two different methods. The basic conclusions obtained from analysis of the two methods are that the assumption that the imaginary (absorption) index can be derived by subtracting Mie-calculated scattering from measured extinction (extinction-matching method) is not necessarily correct, as there is not a unique

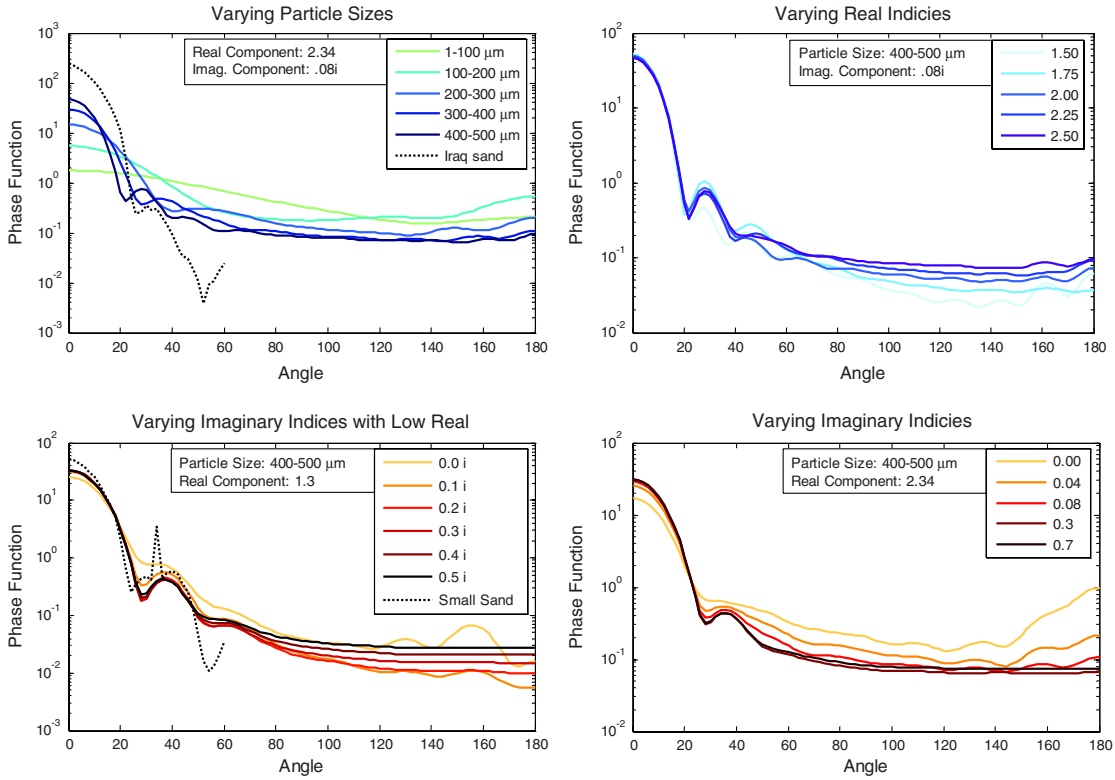

Fig. 11. Clockwise from upper left: Variations in particle size, real index, imaginary index, and imaginary index with a lower real refractive index value. Leftmost plots include an empirically determined phase function for reference; represented as a dotted line. In all cases, the frequency is set at 1 THz.

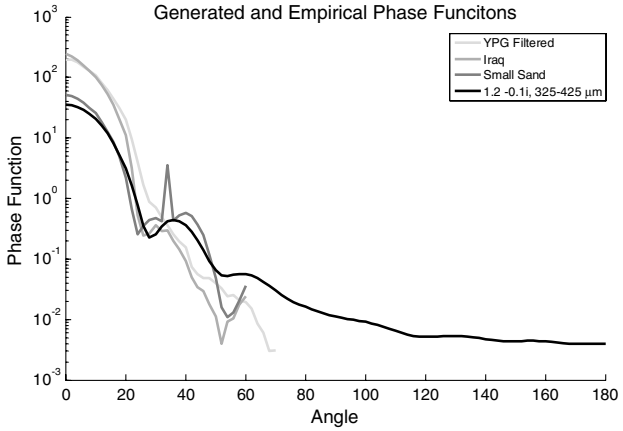

Fig. 12. Three empirical phase functions, in gray, alongside the function predicted by the modified LEEDR model, in black. All functions were evaluated at a frequency of 1 THz.

solution, nor can the real index be calculated without iteration. However, calculating the complex index of refraction from phase angle differences of sample signal and reference phase provides more realistic solutions. Still, this solution suffers in that it also relies on assumptions and is not broad-spectrum—it is tuned specifically for the terahertz portion of the spectrum.

In order to more fully and accurately determine the complete index of refraction, a new experiment was devised in which sample-induced scattering was measured directly through a series of off-axis tests. From this data, a portion of the corresponding scattering phase function was calculated. This empirically determined phase function was compared against one calculated based on Mie theory applied to estimated sample parameters. Through a newly designed interface in LEEDR, five parameters are varied in order to alter the shape of the calculated phase function; at which point that a reasonably close match is formed between the experimental and calculated functions, the input parameters accurately describe the physical properties of the sample, including the real and imaginary components of the CIR. Such a reasonably close match was formed to the samples analyzed in this experiment. The determined real component agrees with the results derived from other methods that utilize terahertz time-domain systems to determine optical parameters, while maintaining a realistically non-zero imaginary component. Additionally, the same process can be applied at any frequency of interest. These results, when completed for the range of 0.1–3 THz, will be implemented into the default LEEDR brownout scenario, and the modified interface will remain a novel tool for correlating a given phase function into physical sample properties.

The views expressed in this paper are those of the authors and do not necessarily reflect the official policy or position of the Air Force, the Department of Defense, or the U. S. government. Wright State University would like to acknowledge the following entities for funding and equipment support: the Ohio Third Frontier Ohio Academic Research Cluster in Layered Sensing, the Institute for the Development and Commercialization of Advanced Sensor Technology, and the Wright State University Office of Research and Sponsored Programs. The Air Force Institute of Technology acknowledges the generous support of the Directed Energy Professional Society (DEPS) and the High Energy Laser Joint Technology Office (HEL-JTO).

References

1. S. T. Fiorino, R. J. Bartell, M. J. Krizo, G. L. Caylor, K. P. Moore, and S. J. Cusumano, "Validation of a worldwide physics-based high-spectral resolution atmospheric characterization and propagation package for UV to RF wavelengths," Proc. SPIE **7090**, 70900I (2008).
2. D. Mittleman, *Sensing with Terahertz Radiation* (Springer, 2002), pp. 1–145.
3. T. W. Crowe, D. W. Porterfield, J. L. Hesler, W. L. Bishop, D. S. Kurtz, and K. Hui, "Terahertz sources and detectors," in *Terahertz for Military and Security Applications III*, R. J. Hwu, D. L. Woolard, and M. J. Rosker, eds., SPIE International Society for Optical Engineering (Bellingham, WA, 2005), pp. 271–280.
4. P. H. Siegel, "Terahertz technology," IEEE Trans. Microwave Theory Tech. **50**, 910–928 (2002).
5. S. L. Marek, "A computational tool for evaluating THz imaging performance in brownout conditions at land sites throughout the world," Master's thesis (Air Force Institute of Technology, 2009).
6. S. T. Fiorino, R. J. Bartell, M. J. Krizo, S. L. Marek, M. J. Bohn, R. M. Randall, and S. J. Cusumano, "A computational tool for evaluating THz imaging performance in brownout conditions at land sites throughout the world," Proc. SPIE **7324**, 732410 (2009).
7. M. Hess, P. Koepke, and I. Schult, "Optical properties of aerosols and clouds: the software package OPAC," Bull. Am. Meteorol. Soc. **79**, 831–844 (1998).
8. M. Naftaly and R. E. Miles, "Terahertz time-domain spectroscopy of silicate glasses and the relationship to material properties," J. Appl. Phys. **102**, 043517 (2007).
9. W. J. Wiscombe, "Improved Mie scattering algorithms," Appl. Opt., **19**, 1505–1510 (1980).
10. S. T. Fiorino, P. M. Grice, M. J. Krizo, R. J. Bartell, J. D. Haiducek, and S. J. Cusumano, "Lab measurements to support modeling terahertz propagation in brownout conditions," Proc. SPIE **7671**, 767131 (2010).
11. M. Van exter and D. R. Grischkowsky, "Characterization of an optoelectronic terahertz beam system," IEEE Trans. Microwave Theory Tech. **38**, 1684–1691 (1990).
12. C. D. Stoik, "Nondestructive evaluation of aircraft composites using terahertz time domain spectroscopy," Ph.D. dissertation (Air Force Institute of Technology, 2008).
13. C. D. Stoik, M. J. Bohn, and J. L. Blackshire, "Nondestructive evaluation of aircraft composites using transmissive terahertz time domain spectroscopy," Opt. Express **16**, 17039–17051 (2008).
14. J. V. Rudd, J. L. Johnson, and D. M. Mittleman, "Quadrupole radiation from terahertz dipole antennas," Opt. Lett. **25**, 1556–1558 (2000).
15. C. Emde, R. Buras, B. Mayer, and M. Blumthaler, "The impact of aerosols on polarized sky radiance: model development, validation, and applications," Atmos. Chem. Phys. **10**, 383–396 (2010).
16. W. Withayachumnankul, B. M. Fischer, H. Lin, and D. Abbott, "Uncertainty in terahertz time-domain spectroscopy measurement," J. Opt. Soc. Am. B **25**, 1059–1072 (2008).